Nanoscale

PAPER

View Article Online
View Journal | View Issue

Cite this: *Nanoscale*, 2019, **11**, 11569

Reduction of Fermi level pinning at Cu–BP interfaces by atomic passivation†

Pengfei Ou,[a] Xiao Zhou,[a,b] Cheng Chen,[a] Fanchao Meng,[a] Yiqing Chen[a] and Jun Song*[a]

Black phosphorus (BP) is a semiconducting material with a direct finite band gap in its monolayer, attracting intense attention for its application in field-effect transistors. However, strong Fermi level pinning (FLP) has been observed for contacts between BP and high work function metals, *e.g.*, Cu. Such FLP presents an undesirable hurdle preventing the achievement of high performance field-effect devices. In this regard, there is a crucial need to understand the FLP occurring at the metal–BP interfaces and explore the possibility to reduce it. The present work studied atomic passivation in reducing FLP for the Cu–BP system using density functional theory calculations. The passivation by H, N, F, S, and Cl atoms on the Cu(111) surface has been considered. The results showed that the passivated atoms can shield the direct contact between Cu(111) and BP, thus reducing FLP at Cu–BP interfaces. In particular, S and Cl atoms were found to be highly effective agents to achieve a significant reduction of FLP, leading to Cu–BP contacts with ultralow Schottky barrier height (SBH) and suggesting the possibility of ohmic contact formation. Our findings demonstrate surface passivation as an effective method towards depinning the Fermi level at the metal–BP interface and subsequently controlling the SBH for BP-based electronic devices.

Received 20th December 2018,
Accepted 7th May 2019

DOI: 10.1039/c8nr10270h

rsc.li/nanoscale

1. Introduction

Following the successful isolation of graphene by micromechanical exfoliation of highly oriented pyrolytic graphite by Novoselov *et al.* in 2004,[1] there has been exponential growth in research studies on two-dimensional (2D) materials. Graphene, a one-atom-thick layer of carbon atoms arranged in a 2D hexagonal crystal lattice, has shown significant promise for its applications in electronic devices due to its intriguing physical, chemical, electrical, mechanical, and thermal properties.[2] However, the absence of either an electronic band gap or a controllable method to create this gap without altering the outstanding properties of graphene has limited its applications. Recently, a new class of 2D materials, *i.e.*, monolayer black phosphorus (BP), namely phosphorene, has shown promise to address the aforementioned limitations. First-principles calculations have demonstrated that it exhibits a highly tunable band gap that changes with the number of layers from 0.91 eV for monolayer to 0.28 eV for five-layer BP.[3] Li *et al.*[4] showed that thickness-dependent and highly anisotropic field-effect mobility values up to 1000 $cm^2 V^{-1} s^{-1}$ can be achieved using few-layer BP field-effect transistors (FETs). Contrary to the multilayer transition metal dichalcogenides (TMDCs) that exhibit an indirect band gap,[5] multilayer BP has a direct band gap, which is beneficial for electronic and optoelectronic applications.[6–8] In addition to these characteristics, monolayer BP has also been shown to possess other attractive features, such as strong in-plane anisotropy,[9] layer-dependent on/off ratio and carrier mobility.[10]

A metal–semiconductor interface (MSI) is a critical component affecting the performance of electronic and optoelectronic devices. Being one of the most significant parameters that determine the electronic characteristics of the metal–semiconductor contact, the Schottky barrier height (SBH) refers to the energy which must be provided for charge carriers to transport across the junction.[11,12] The apparent importance of SBH to the semiconductor industry has led to tremendous theoretical and experimental efforts to understand its formation mechanism and to seek the means of controlling or tuning the SBH at the MSI. Specifically, for the metal–BP interface, numerous studies have been performed to examine BP-based FETs with a variety of metal electrodes.[4,10,13–21] It was found that the behaviors of metal–BP interfaces depend on both the selection of metal electrodes and the thickness of channel BP.[4,14–16] In one pioneering study by Li *et al.*[4] on BP FETs, the Schottky barrier formation at the metal–BP interface

[a]*Department of Mining and Materials Engineering, McGill University, Montreal, Quebec, Canada H3A 0C5. E-mail: jun.song2@mcgill.ca; Fax: +1 (514) 398-4492; Tel: +1 (514) 398-4592*
[b]*Institute of Mechanical Engineering, École Polytechnique Fédérale de Lausanne, Lausanne, Vaud, Switzerland CH-1015*

†Electronic supplementary information (ESI) available. See DOI: 10.1039/c8nr10270h

for electron injection was detected, and BP was shown to behave as ambipolar FETs when in contact with Cr/Au and Ti/Au electrodes. Du *et al.*[14] confirmed the nature of BP transistors as being Schottky barrier FETs when BP comes into contact with Ni and Pd electrodes, where the device demonstrates more pronounced ambipolar behaviors with the Ni electrode attributed to a weak FLP at the metal–BP interface. Perello *et al.*[15] found different characteristics of BP FETs by varying contact-metal and thickness engineering. A unipolar to ambipolar transition was demonstrated as the thickness increases with Al contacts. Meanwhile, a p-type to ambipolar transition was observed as the thickness of BP decreases with Pd contacts, contrary to the findings by Du *et al.*[14] Few-layer BP FETs with Ti and Pd electrodes under various gate-bias conditions were studied by Das *et al.*[16] and it was shown that the Ti electrode provides a smaller SBH for electron injection. Additionally, a p-type BP FET device was realized using Ti/Au electrodes and a Schottky barrier formation was also detected at the metal–BP interface for hole injection by Liu *et al.*[10] The Schottky barrier formation on metal–BP contacts has also been demonstrated by various theoretical density functional theory (DFT) calculations. Pan *et al.*[17] found that monolayer BP exhibits a p-type Schottky barrier when it comes into contact with Ti, Ni, and Pd electrodes and an n-type Schottky barrier when it forms the contact with Al, Cr, Cu, Ag, and Au electrodes. Maity *et al.*[19] studied the adsorption of metal atoms on monolayer BP and demonstrated Ti as a good metal electrode material in monolayer BP devices. Zhu *et al.*[20] revealed that ohmic contacts can be formed between monolayer BP and Cu(111) and Ag(111), and contacts of this nature have also been confirmed by Chanana *et al.*[21] between monolayer BP and Pd(111) and Ti(0001).

Ideally, the SBH would be governed by the work function of metal electrodes according to the Schottky–Mott rule. However, the actual junction is nearly unfailingly a Schottky barrier, with the Fermi level "pinned" deep in the semiconductor band gap at the interface, namely the Fermi level pinning (FLP).[22] The existence of the FLP can be attributed to a few causes,[12] including interface dipoles,[12,23–25] metal-induced gap states (MIGS),[23,26–28] formation of defects at the interface, occurrence of chemical reactions and existence of lattice distortion.[11,12,29,30] Strong FLP ensures the absence of a strong dependency of SBH on the work function of metals, and thus SBH being rather inaccessible to tuning by using different metal electrodes, which obstructs the realization of ohmic contacts and hinders the applications of BP in FET devices. As such, FLP has been a subject of intense research[13,30–34] and various methods of reducing FLP at the MSI have been proposed, such as atom-passivation,[31] insertion of ultrathin materials,[32,33] usage of 2D metal electrodes,[34] and thermal annealing.[13]

The present study focuses on the means of atom-passivation in reducing FLP at the Cu–BP contact. Here, Cu is designated as the metal electrode as Cu(111) has been shown to be a promising candidate to form an excellent ohmic contact with monolayer BP.[35] The passivation of Cu(111) by hydrogen (H), nitrogen (N), fluorine (F), sulfur (S), and chlorine (Cl) atoms is considered. DFT calculations were performed to examine the atomic and electronic structures of atom-passivated Cu–BP interfaces. The potency of different passivating atoms in reducing the FLP has been analyzed and explained. It is found that S- and Cl-passivation can significantly weaken the interfacial interaction to induce the formation of the ohmic contact. Our results demonstrate atom-passivation as a feasible method to achieve SBH tuning for metal–BP interfaces.

2. Computational methods

DFT calculations were performed within generalized gradient approximation (GGA) for exchange–correlation functionals[36,37] implemented in the Vienna *ab initio* simulation package (VASP)[38,39] to examine the Cu–BP interfaces. The electron–ion interactions were represented by the projector-augmented wave (PAW) pseudopotentials,[40,41] and van der Waals (vdW) corrections were incorporated using Grimme's DFT-D2 method based on a semi-empirical GGA-type theory.[42] A vacuum buffer space of more than 20 Å in thickness was set to avoid spurious interaction between periodic images. The cut-off energy was set to 400 eV for the plane wave basis set, and $(4 \times 4 \times 1)$ and $(6 \times 6 \times 1)$ Monkhorst–Pack *k*-point mesh grids[43] were used for atomic optimization and self-consistent calculations, respectively. Benchmark tests were conducted to confirm that the cut-off energy and *k*-point mesh grids yield sufficient accuracy and good convergence. Atomic coordinates were fully optimized until the Hellmann–Feynman forces are less than 0.01 eV $Å^{-1}$.

The Cu–BP system comprises a monolayer BP interfacing with a Cu slab that exhibits the (111) surface orientation, the preferred orientation of the Cu surface[44] with the lowest surface energy,[45,46] as illustrated in Fig. 1. The Cu slab model consists of a (4×4) surface unit cell of 6 atomic layers. The top Cu surface interfacing with the BP is either in its pristine state or atom-passivated by H, N, F, S, and Cl atoms (more details about metrics for selecting these passivating atoms can be found in the ESI†). Benchmark calculations have been performed to confirm that the slab thickness is sufficient to achieve converged results of the contact properties. The monolayer BP has a (3×2) unit cell. The in-plane lattice constants of pristine and atomic-passivated Cu(111) surfaces were adjusted to match the ideal lattice constants of BP to obtain the exact band alignment in BP. This treatment also maintains BP in a pseudo strain-free state as its electronic properties are remarkably sensitive to strain. In all the Cu–BP interfaces, all the atoms were allowed to relax except for the bottom two layers of the Cu(111) slab, which were fixed during calculations.

3. Results and discussion

3.1 *Ab initio* electronic structure calculations

The isolated monolayer BP was first examined as the reference system and to benchmark the settings of our calculations. The optimized lattice constants of the monolayer BP were determined to be $a = 4.57$ Å and $b = 3.31$ Å along the x and y direc-

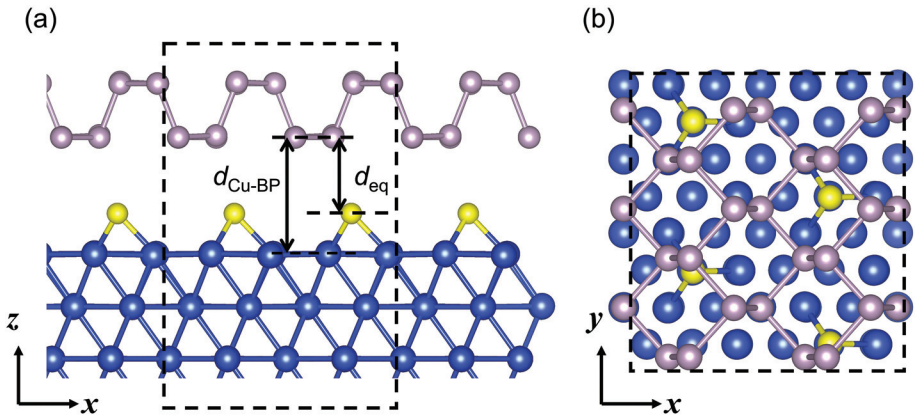

Fig. 1 (a) Side and (b) top views of the atomic structure of BP adsorbed on the atom-passivated (H, N, F, S, and Cl atoms) Cu(111) surface. Unit cells are indicated by black dashed lines both in (a) and (b). Purple and blue spheres represent P and Cu atoms, respectively, while yellow spheres indicate the passivating atoms on Cu(111).

tions, respectively (Fig. 1), in excellent agreement with the values reported in the literature.[17,19,21,35,47,48] Generally speaking, there are four kinds of commonly used band gaps for a 2D semiconductor: transport gap (a sum of the SBH for electrons and holes), quasiparticle band gap (dominated by many-electron effects), optical gap (dominated by exciton effects), and DFT band gap (single electron approximation). For monolayer BP, four kinds of band gaps were reported as 1.0,[49] 2.0,[6] 1.3–1.45,[10,50] and 0.91 (PBE functional) eV,[17] respectively. Even though the PBE functional is well-known for systematically underestimating the band gap of semiconductors, the DFT band gap is closest to the transport SBH because many-electron effects have been strongly suppressed due to charge doping of channel monolayer BP by a metal source/drain electrode or gate electrode.[17] The monolayer BP was found to exhibit a direct band gap of 0.89 eV, with the valence band minimum (VBM) and conduction band minimum (CBM) exactly at the Γ point of the first Brillouin-zone, also in agreement with previous theoretical calculations.[19] In addition, the work function was calculated to be 4.72 eV, in line with the value of 4.50 eV previously reported by Cai *et al.*[51]

The structural and electronic properties of the Cu–BP interfaces (*cf.* Fig. 1) are listed in Table 1. The binding energy (E_b) of the Cu–BP contact (per surface unit cell) is defined as

$$E_b = E_{Cu} + E_{BP} - E_{Cu-BP} \quad (1)$$

where E_{Cu}, E_{BP}, and E_{Cu-BP} are the energies of the pristine or atom-passivated Cu(111) substrate and pristine BP, and the total energy of BP on the pristine and atom-passivated Cu(111) surface, respectively. When the Cu surface is passivated, the passivating atoms (H, N, F, S, and Cl) were found to adsorb preferentially on the fcc sites of Cu(111), as also confirmed by previous studies.[52–62] Consequently, the atomic configurations with passivating atoms adsorbed on the most stable fcc sites of Cu(111) were considered in our calculations. Fig. 1(a) and (b) show the side and top views of a monolayer BP sheet interfacing with the atom-passivated Cu(111).

Table 1 Structural and electronic properties of monolayer BP on pristine or atom-passivated Cu(111)

	W^a (eV)	$d_{Cu-BP}{}^b$ (Å)	$d_{eq}{}^c$ (Å)	$E_b{}^d$ (eV per surface unit cell)	VBM^e (eV)	CBM^f (eV)	$D_{it}{}^g$ (# of states cm^{-2} eV)
Cu	4.89	2.25	—	8.75	−0.54	0.25	1.78×10^{14}
H/Cu	4.90	2.39	1.74	7.01	−0.58	0.23	1.49×10^{14}
N/Cu	5.22	2.31	1.33	7.65	−0.38	0.45	1.67×10^{14}
F/Cu	5.14	2.98	1.75	3.30	−0.18	0.62	7.20×10^{13}
S/Cu	5.10	4.56	2.97	1.24	−0.03	0.84	2.50×10^{13}
Cl/Cu	5.08	4.98	3.15	0.94	−0.01	0.85	1.88×10^{13}

[a] Work function (W) of pristine (or atom-passivated) Cu(111). [b] Average separation (d_{Cu-BP}) between Cu and BP. [c] Average separation (d_{eq}) between the passivating atoms and BP. [d] Binding energy (E_b) between pristine (or atom-passivated Cu) and BP. [e] Valence band maximum (VBM) of BP in the Cu–BP heterojunction. [f] Conduction band minimum (CBM) of BP in the Cu–BP heterojunction. [g] Interfacial trap density (D_{it}).

After optimization, the key structural and electronic properties of the monolayer BP on the pristine or atom-passivated Cu(111) substrate are obtained and enlisted in Table 1. Here, the parameter d_{Cu-BP} is defined as the average separation between the top Cu surface and monolayer BP, and d_{eq} denotes the average separation between the passivating atoms and monolayer BP, as illustrated in Fig. 1. As seen in Table 1, d_{Cu-BP} is increased by the presence of passivating atoms, while d_{eq} is generally less than the distance between the pristine Cu and BP (2.25 Å), except for S- and Cl-passivated Cu due to the larger atomic radii of S and Cl atoms. Examining the binding energy E_b (see eqn (1)), we see that overall passivation weakens the bonding strength between BP and Cu, resulting in decreased E_b. In addition, a clear negative correlation between E_b and d_{Cu-BP} can be observed, suggesting that such weakening can be attributed to the fact that the passivating atoms reduce the direct interaction between Cu and BP by increasing their separation. Depending on the value of E_b, the Cu–BP interfaces

can be classified into three categories: weak bonding (S and Cl) with E_b = 0.94–1.24 eV, medium bonding (F) with E_b = 3.30 eV, and strong bonding (H and N) with E_b = 7.01–7.65 eV. Particularly, we see that S or Cl passivation results in nearly an order of magnitude reduction in the bonding energy, hinting a significant reduction of the FLP effect at Cu–BP interfaces.

The partial density of states (PDOS) data of monolayer BP on pristine and atom-passivated Cu(111) at the equilibrium position have been examined for a detailed analysis of the reduction of FLP at Cu–BP interfaces, as depicted in Fig. 2. The black solid lines in the plots indicate PDOS of the monolayer BP, while the vertical orange dashed lines indicate the associated VBM and CBM. The VBM and CBM of BP are determined through the projected BP states at the Γ point, with their exact locations listed in Table 1. As seen from Fig. 2, the proximity to the metal substrate renders all metal–BP interfaces metallic, in agreement with previously published results on metal–BP contacts.[17–19,21,35,63] If there is no FLP at Cu–BP interfaces, then Cu with a relatively large work function (4.89 eV) would have a p-type contact with BP. However, it has been shown that Cu forms an n-type contact with BP, despite its high work function.[21,26,27] Our calculations also confirm that the Fermi level is "pinned" deeply in the semiconductor band gap and close to the CBM, representing the n-type contact as shown in Fig. 2(a) and Table 1. This evidences the occurrence of a strong FLP at the Cu–BP interfaces. Fig. 2(b)–(f) illustrate the calculated PDOSs of adsorbed BP on H-, N-, F-, S-, and Cl-passivated Cu(111) surfaces. We see that atom-passivated Cu(111) may exhibit a work function ranging from 4.89 to 5.22 eV depending on the types of passivating atoms, as summarized in Table 1. Unlike the pristine Cu–BP contact, BP shows a p-type contact with atom-passivated Cu(111), except for the case of H-passivation. Particularly notable is that the adsorbed BP on S- and Cl-passivated Cu(111) exhibits a Fermi level almost located at its VBM (*cf.* Fig. 2(e) and (f)), and that S- and Cl-passivated Cu(111) surfaces present near-zero p-type SBHs (0.03 eV and 0.01 eV respectively, *cf.* Table 1), indicative of possible ohmic contact formation and low finite barriers for electron injection.

The significant reduction of FLP by S- and Cl-passivation is possibly attributed to the strong ability of S and Cl atoms in weakening the direct interaction between Cu and BP by increasing their separation (*cf.* Table 1). To confirm this hypothesis, we constructed the corresponding Cu–BP contact model, where BP is manually placed at 6 Å away from the pristine or atom-passivated Cu(111). The corresponding PDOS plots are indicated by gray shaded regions in Fig. 2. At the distance of 6 Å, there is negligible direct interaction between Cu(111) and BP, and no metal-induced gap states are observed in the PDOS of adsorbed BP. In the case of pristine and H-passivated Cu in Fig. 2(a) and (b), PDOS indicated by the gray shaded regions is shifted about 0.28 eV with respect to that indicated by black solid line regions. Such a difference between the PDOSs of BP at 6 Å away and at the equilibrium distance from the pristine and H-passivated Cu(111) surface can be evidence for a strong FLP at the Cu–BP interfaces. A similar behavior is also observed in the case of adsorbed BP on N- and F-passivated Cu(111) surfaces. However, as depicted in Fig. 2(e) and (f), PDOSs of BP at the equilibrium position almost coincide with those of BP at 6 Å away from the Cu(111) surface, irrespective of the change in work function. This indicates that the FLP effect is reduced at the Cu–BP interfaces due

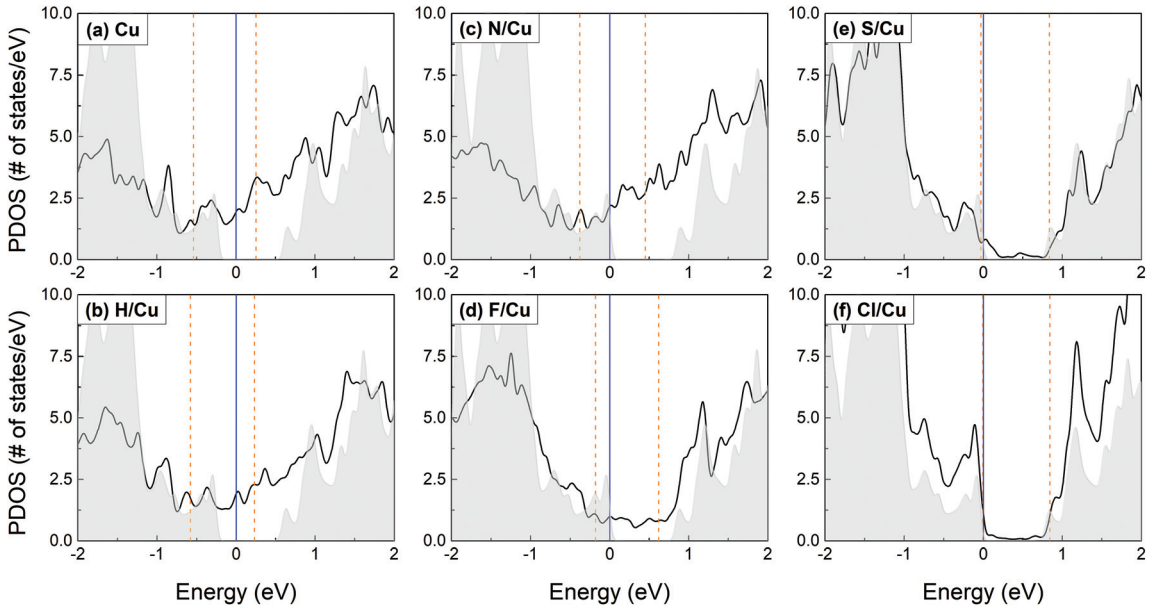

Fig. 2 Partial density of states (PDOS) for adsorbed BP on (a) pristine, (b) H-, (c) N-, (d) F-, (e) S-, and (f) Cl-passivated Cu(111) surfaces, with black solid lines representing PDOS and orange dashed lines indicating VBM and CBM of BP at d_{eq} from pristine or atom-passivated Cu(111). The gray shaded regions denote corresponding PDOS plots of BP at about 6 Å separation from pristine or atom-passivated Cu(111). Blue solid line indicates the Fermi level (E_F) at d_{eq} and is set to 0 eV.

to the passivating S and Cl atoms, avoiding the direct contact (or interaction) between BP and Cu(111).

3.2 Quantitative estimation of the degree of FLP reduction

Weakened interaction between Cu(111) and BP with passivating atoms induces a decrease of gap states and thus a reduction of FLP at Cu–BP interfaces. For a quantitative estimation of the reduction in FLP by passivating atoms, the calculated interfacial trap density (D_{it}) is measured using the following equation at the equilibrium position, summarized in Table 1,

$$D_{it} = \left(\int_{VBM}^{CBM} D(E)\mathrm{d}E\right)/(\square a \cdot \text{unit energy}) \quad (2)$$

here, $D(E)$ and $\square a$ are the density of states for adsorbed BP and interfacial surface area, respectively. In the present study, the interfacial area is around $\sim 9.09 \times 10^{-15}$ cm^2. When BP is adsorbed on pristine Cu(111), $D_{it} = 1.78 \times 10^{14}$ (# of states per cm^2 eV) is obtained. This D_{it} value can decrease in the presence of passivating atoms on substrates leading to the weakened interaction between BP and atom-passivated Cu(111). Thus, D_{it} is generally decreased at atom-passivated Cu–BP interfaces, as shown in Table 1. Particularly, when BP is adsorbed on S- and Cl-passivated Cu(111), D_{it} evidently decreases to the smallest values of 2.50×10^{13} and 1.88×10^{13} (# of states per cm^2 eV).

One of the reasons for FLP is related to the interface dipole formation due to charge redistribution at the MSI. Fig. 3(a)–(f) depict the plane-averaged charge density difference (Δn) of BP on pristine, H-, N-, F-, S-, and Cl-passivated Cu(111), respectively, where the charge density change after the junction formation is determined using the following equation:

$$\Delta n = n_{Cu-BP} - (n_{Cu} + n_{BP}) \quad (3)$$

here, n_{Cu}, n_{BP}, and n_{Cu-BP} are the plane-averaged charge density of isolated Cu(111), isolated BP, and BP on pristine or atom-passivated Cu(111), respectively. Red and blue regions in Fig. 3 indicate the charge accumulation and depletion, respectively, while interfacial regions of pristine or atom-passivated Cu–BP are colored in yellow. An asymmetric distribution of charge accumulation/depletion is observed between the interface of pristine (or atom-passivated) Cu surface and BP, indicating the formation of an interface dipole. The interface dipole is capable of shifting the electronic energy levels from the original positions, and thus renders a deviation from the Schottky–Mott rule. However, charge redistribution at the atom-passivated Cu–BP interfaces is reduced compared to that of the pristine Cu–BP interface. In particular, a negligible charge redistribution occurs at S- and Cl-passivated Cu–BP interfaces, which leads to the smallest interface dipole formation and agrees well with the aforementioned results representing weakened interaction by passivating atoms.

To further quantitatively evaluate the effect of FLP, the exact locations of VBM and CBM of adsorbed BP on different substrates are analyzed, as depicted in Fig. 4. The white and gray bars in Fig. 4 respectively indicate the energy ranges from VBM to CBM of BP located at the equilibrium separation and 6 Å from the pristine or atom-passivated Cu(111) substrates. Meanwhile, the ideal locations of VBM and CBM are also determined, solely by the work function difference without direct interaction between BP and Cu(111), *i.e.*, according to the Schottky–Mott rule. Within the Schottky–Mott rule, ideal locations of VBM and CBM are governed by the following equations:

$$\text{VBM}_{ideal} = -(E_g/2 - (W_{Cu} - W_{BP}) \quad (4)$$

$$\text{CBM}_{ideal} = E_g + \text{VBM}_{ideal} \quad (5)$$

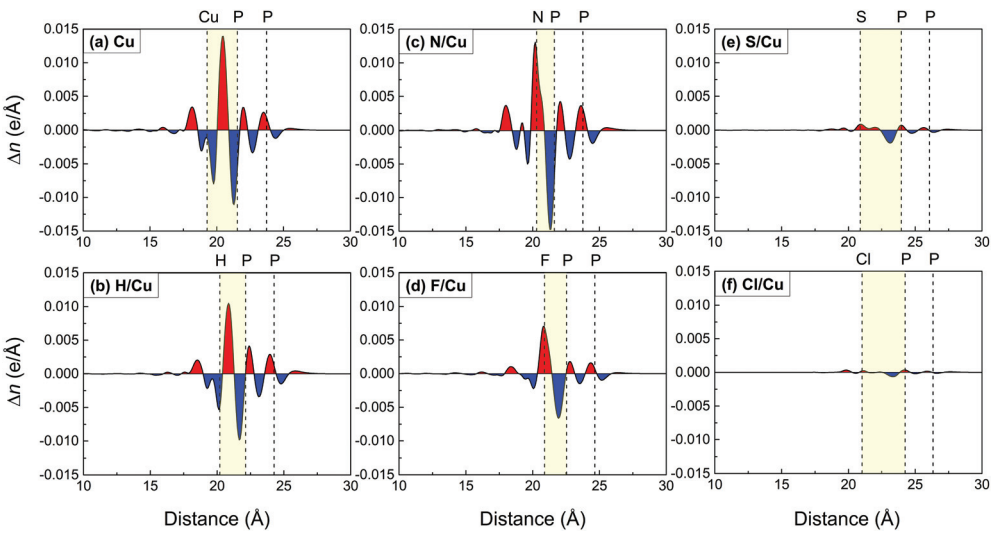

Fig. 3 Plane-averaged charge density difference (Δn) of BP on (a) pristine, (b) H-, (c) N-, (d) F-, (e) S-, and (f) Cl-passivated Cu(111). Red/blue regions indicate the charge accumulation/depletion, respectively. The regions of pristine or atom-passivated Cu–BP interfaces are shaded in yellow.

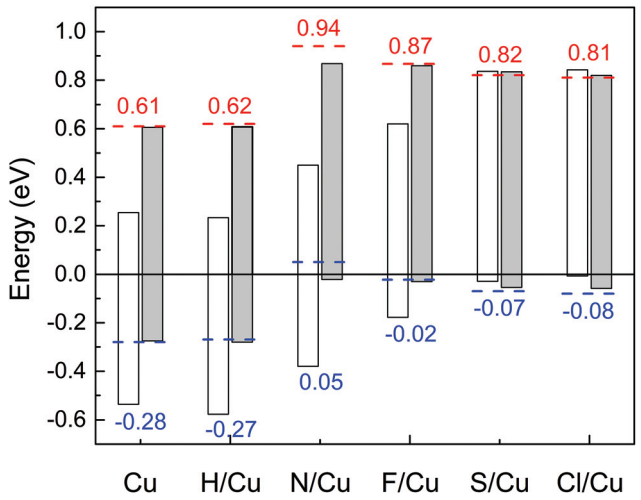

Fig. 4 Locations of valence band maximum (VBM) to conduction band minimum (CBM) with reference to the Fermi level of adsorbed BP on pristine and atom-passivated Cu(111) substrates. White and gray bars indicate the VBM–CBM ranges for adsorbed BP at d_{eq} and at 6 Å from Cu(111), respectively. Blue and red dashed lines indicate the ideal positions of VBM and CBM predicted from the Schottky–Mott rule, respectively.

where E_g, W_{Cu}, and W_{BP} refer to the band gap of isolated BP, the work functions of pristine or atom-passivated Cu(111) and isolated BP, respectively. The ideal locations of VBM and CBM, calculated from eqn (4) and (5), are indicated by blue and red dashed lines, respectively, in Fig. 4. We can see that these ideal locations lie close to (within 0.1 eV margin) the ones obtained for BP at 6 Å separation from the Cu substrate, except for the case of N-passivated Cu surface. In the N-passivated case, the locations of BP are converged to the ideal values of VBM and CBM, when the separation between BP and the N-passivated Cu surface is around at 8 Å, similar to the case of adsorbed MoS_2 on the N-passivated Au surface.[31] This close match indicates the good applicability of the Schottky–Mott rule in accurately describing weakly interacting BP–metal contacts. On the other hand, on examining the cases of equilibrium BP absorption on different Cu substrates, we see that the Schottky–Mott rule fails to correctly predict the VBM and CBM locations, except for BP adsorbed on S- and Cl-passivated Cu substrates. This further evidences the effectiveness of S and Cl in weakening the interaction at the BP–Cu interface to moderate Fermi level pinning, confirming atom-passivation as a potential pathway to control the SBH for BP-based electronic devices.

3.3 Discussion

The Fermi level unpinning achieved by atomic passivation is essentially attributed to the passivating atoms weakening the interfacial interaction and modifying the metal work functions. Passivating atoms effectively create an air or vdW gap between the semiconductor and metal, act as a buffer layer to block the penetration of electron waves from metal electrodes, and therefore significantly reduce the overlapped molecular orbitals and chemical bonds, thus suppressing MIGS and weakening FLP. As such, passivating atoms on the metal surface provide a possible means to solve the FLP issue in the pristine semiconductor–metal junction, thus potentially achieving an "ideal" junction that would be governed by the Schottky–Mott rule. This would also enable the prediction of the SBH of the semiconductor–metal junction by knowing the metal work function after atomic passivation. On the other hand, the addition of a layer of passivating atoms at the interface decouples the direct interaction between the metal and semiconductor and might actually result in a reduction in the current flow at the junction, despite the fact that passivating atoms reduce the actual band offset between the metal and semiconductor majority band. This is directly correlated with the tunneling efficiency, which would drop exponentially with the thickness of the layer gap.[12] Such an effect may also be quantified by the total transmission coefficient, which can be evaluated employing the non-equilibrium Green's function (NEGF) approach[64] combined with DFT calculations and the WKB approximation.[65]

The method of atom passivation is also in accordance with previous studies, which employed the vdW-type electrical contact[34,66,67] or a physical interfacial layer in between the semiconductor–metal junction[33,68–70] to decrease the SBH. The atom passivation method is expected to be a generic one that may be applied to metal electrodes other than Cu (see the case study of the Ni electrode in the ESI†). However, the usage of a different metal electrode necessarily confers different characteristics to the MSI, and consequently, the effectiveness of a passivating species in Fermi level unpinning may vary. Therefore, it would be of critical importance to establish the criteria/guidelines in the identification and selection of candidate passivating atoms, which is certainly worthy of further studies.

Despite the demonstrated effectiveness of atom passivation in Fermi level unpinning, it is worth noting that the realization of the method would demand preferential and stable bonding of the passivating atoms with the metal surface at the MSI, in order to avoid random introduction of dopants/adatoms to induce unwanted alteration of the electronic properties of the semiconductor (*i.e.*, BP in the present study). This not only requires the passivating atoms to exhibit strong binding with the metal yet weak interaction with the semiconductor but also precise location control for the passivating atoms during processing, a challenge necessitating consideration in practical applications.

4. Conclusions

In summary, the present study investigated atom passivation as a method to reduce Fermi level pinning (FLP) at the Cu–BP interfaces using density functional theory calculations. Several candidate atoms, H, N, F, S, and Cl, passivating the surface of Cu(111), have been examined. It is found that the passivating

atoms may shield direct contact between pristine Cu(111) and BP, therefore inducing a weakened interaction between atom-passivated Cu(111) and BP. In particular, S and Cl atoms greatly reduce FLP at Cu–BP interfaces, evidenced by fewer metal-induced gap states, reduced interfacial trap density, and negligible interfacial charge redistribution. Intriguingly, S- or Cl-passivated Cu–BP contacts exhibit an ultralow SBH smaller than 0.1 eV, suggesting the possibility of ohmic contact formation. The findings confirm the effectiveness of atom passivation in FLP reduction and identify important metrics to provide guidelines for depinning the Fermi level at the MSI so that the control of SBH for the BP-based electronic devices can be possibly achieved.

Conflicts of interest

The authors declare no conflicts of interest.

Acknowledgements

This research is supported by the NSERC Discovery grant (grant # RGPIN-2017-05187), the NSERC Strategic grant (grant # STPGP 494012-16), and the McGill Engineering Doctoral Award (MEDA). The authors would also like to acknowledge the Supercomputer Consortium Laval UQAM McGill and Eastern Quebec for providing computing resources.

References

1 K. S. Novoselov, A. K. Geim, S. V. Morozov, D. Jiang, Y. Zhang, S. V. Dubonos, I. V. Grigorieva and A. A. Firsov, *Science*, 2004, **306**, 666–669.
2 M. J. Allen, V. C. Tung and R. B. Kaner, *Chem. Rev.*, 2009, **110**, 132–145.
3 J. Qiao, X. Kong, Z.-X. Hu, F. Yang and W. Ji, *Nat. Commun.*, 2014, **5**, 4475.
4 L. Li, Y. Yu, G. J. Ye, Q. Ge, X. Ou, H. Wu, D. Feng, X. H. Chen and Y. Zhang, *Nat. Nanotechnol.*, 2014, **9**, 372–377.
5 J. K. Ellis, M. J. Lucero and G. E. Scuseria, *Appl. Phys. Lett.*, 2011, **99**, 261908.
6 V. Tran, R. Soklaski, Y. Liang and L. Yang, *Phys. Rev. B: Condens. Matter Mater. Phys.*, 2014, **89**, 235319.
7 A. S. Rodin, A. Carvalho and A. H. Castro Neto, *Phys. Rev. Lett.*, 2014, **112**, 176801.
8 T. Low, A. S. Rodin, A. Carvalho, Y. Jiang, H. Wang, F. Xia and A. H. Castro Neto, *Phys. Rev. B: Condens. Matter Mater. Phys.*, 2014, **90**, 075434.
9 F. Xia, H. Wang and Y. Jia, *Nat. Commun.*, 2014, **5**, 4458.
10 H. Liu, A. T. Neal, Z. Zhu, Z. Luo, X. Xu, D. Tománek and P. D. Ye, *ACS Nano*, 2014, **8**, 4033–4041.
11 S. M. Sze and K. K. Ng, *Physics of Semiconductor Devices*, John Wiley & Sons, 2006.
12 R. T. Tung, *Appl. Phys. Rev.*, 2014, **1**, 011304.
13 Z.-P. Ling, S. Sakar, S. Mathew, J.-T. Zhu, K. Gopinadhan, T. Venkatesan and K.-W. Ang, *Sci. Rep.*, 2015, **5**, 18000.
14 Y. Du, H. Liu, Y. Deng and P. D. Ye, *ACS Nano*, 2014, **8**, 10035–10042.
15 D. J. Perello, S. H. Chae, S. Song and Y. H. Lee, *Nat. Commun.*, 2015, **6**, 7809.
16 S. Das, M. Demarteau and A. Roelofs, *ACS Nano*, 2014, **8**, 11730–11738.
17 Y. Pan, Y. Wang, M. Ye, R. Quhe, H. Zhong, Z. Song, X. Peng, D. Yu, J. Yang, J. Shi and J. Lu, *Chem. Mater.*, 2016, **28**, 2100–2109.
18 Y. Pan, Y. Dan, Y. Wang, M. Ye, H. Zhang, R. Quhe, X. Zhang, J. Li, W. Guo, L. Yang and J. Lu, *ACS Appl. Mater. Interfaces*, 2017, **9**, 12694–12705.
19 A. Maity and P. Sen, *Int. J. Mod. Phys. B*, 2017, **31**, 1750077.
20 S. Zhu, Y. Ni, J. Liu and K. Yao, *J. Phys. D: Appl. Phys.*, 2015, **48**, 445101.
21 A. Chanana and S. Mahapatra, *J. Appl. Phys.*, 2014, **116**, 204302.
22 F. Léonard and J. Tersoff, *Phys. Rev. Lett.*, 2000, **84**, 4693.
23 C. Gong, L. Colombo, R. M. Wallace and K. Cho, *Nano Lett.*, 2014, **14**, 1714–1720.
24 R. T. Tung, *Phys. Rev. B: Condens. Matter Mater. Phys.*, 2001, **64**, 205310.
25 T. Iffländer, S. Rolf-Pissarczyk, L. Winking, R. Ulbrich, A. Al-Zubi, S. Blügel and M. Wenderoth, *Phys. Rev. Lett.*, 2015, **114**, 146804.
26 Y. Guo, D. Liu and J. Robertson, *ACS Appl. Mater. Interfaces*, 2015, **7**, 25709–25715.
27 J. Kang, W. Liu, D. Sarkar, D. Jena and K. Banerjee, *Phys. Rev. X*, 2014, **4**, 031005.
28 I. Popov, G. Seifert and D. Tománek, *Phys. Rev. Lett.*, 2012, **108**, 156802.
29 J. Su, L. Feng, Y. Zhang and Z. Liu, *Nanotechnology*, 2017, **28**, 105204.
30 Y. Liu, P. Stradins and S. H. Wei, *Angew. Chem.*, 2016, **128**, 977–980.
31 K.-A. Min, J. Park, R. M. Wallace, K. Cho and S. Hong, *2D Mater.*, 2016, **4**, 015019.
32 T. Nishimura, K. Kita and A. Toriumi, *Appl. Phys. Express*, 2008, **1**, 051406.
33 B.-Y. Tsui and M.-H. Kao, *Appl. Phys. Lett.*, 2013, **103**, 032104.
34 Y. Y. Liu, P. Stradins and S. H. Wei, *Sci. Adv.*, 2016, **2**, e1600069.
35 K. Gong, L. Zhang, W. Ji and H. Guo, *Phys. Rev. B: Condens. Matter Mater. Phys.*, 2014, **90**, 125441.
36 W. Kohn and L. J. Sham, *Phys. Rev.*, 1965, **140**, A1133–A1138.
37 J. P. Perdew, K. Burke and M. Ernzerhof, *Phys. Rev. Lett.*, 1996, **77**, 3865–3868.
38 G. Kresse and J. Furthmüller, *Phys. Rev. B: Condens. Matter Mater. Phys.*, 1996, **54**, 11169–11186.
39 G. Kresse and J. Furthmüller, *Comput. Mater. Sci.*, 1996, **6**, 15–50.
40 P. E. Blöchl, *Phys. Rev. B: Condens. Matter Mater. Phys.*, 1994, **50**, 17953–17979.

41 G. Kresse and D. Joubert, *Phys. Rev. B: Condens. Matter Mater. Phys.*, 1999, **59**, 1758–1775.
42 S. Grimme, J. Antony, S. Ehrlich and H. Krieg, *J. Chem. Phys.*, 2010, **132**, 154104.
43 H. J. Monkhorst and J. D. Pack, *Phys. Rev. B: Condens. Matter Mater. Phys.*, 1976, **13**, 5188–5192.
44 T. Hsu and J. M. Cowley, *Ultramicroscopy*, 1983, **11**, 239–250.
45 H. L. Skriver and N. M. Rosengaard, *Phys. Rev. B: Condens. Matter Mater. Phys.*, 1992, **46**, 7157–7168.
46 I. Galanakis, N. Papanikolaou and P. H. Dederichs, *Surf. Sci.*, 2002, **511**, 1–12.
47 R. Quhe, X. Peng, Y. Pan, M. Ye, Y. Wang, H. Zhang, S. Feng, Q. Zhang, J. Shi, J. Yang, D. Yu, M. Lei and J. Lu, *ACS Appl. Mater. Interfaces*, 2017, **9**, 3959–3966.
48 P. Ou, P. Song, X. Liu and J. Song, *Adv. Theory Simul.*, 2019, **2**, 1800103.
49 S. Das, W. Zhang, M. Demarteau, A. Hoffmann, M. Dubey and A. Roelofs, *Nano Lett.*, 2014, **14**, 5733–5739.
50 X. Wang, A. M. Jones, K. L. Seyler, V. Tran, Y. Jia, H. Zhao, H. Wang, L. Yang, X. Xu and F. Xia, *Nat. Nanotechnol.*, 2015, **10**, 517.
51 Y. Cai, G. Zhang and Y.-W. Zhang, *Sci. Rep.*, 2014, **4**, 6677.
52 S. Peljhan and A. Kokalj, *J. Phys. Chem. C*, 2009, **113**, 14363–14376.
53 I. A. Pašti and S. V. Mentus, *Electrochim. Acta*, 2010, **55**, 1995–2003.
54 T. Roman and A. Groß, *Phys. Rev. Lett.*, 2013, **110**, 156804.
55 D. R. Alfonso, A. V. Cugini and D. S. Sholl, *Surf. Sci.*, 2003, **546**, 12–26.
56 I. A. Pašti, N. M. Gavrilov and S. V. Mentus, *J. Serb. Chem. Soc.*, 2013, **78**, 1763–1773.
57 G.-C. Wang, L. Jiang, X.-Y. Pang and J. Nakamura, *J. Phys. Chem. B*, 2005, **109**, 17943–17950.
58 A. Soon, L. Wong, M. Lee, M. Todorova, B. Delley and C. Stampfl, *Surf. Sci.*, 2007, **601**, 4775–4785.
59 K. Nobuhara, H. Nakanishi, H. Kasai and A. Okiji, *Surf. Sci.*, 2001, **493**, 271–277.
60 J. L. Nie, H. Y. Xiao and X. T. Zu, *Chem. Phys.*, 2006, **321**, 48–54.
61 P. Ferrin, S. Kandoi, A. U. Nilekar and M. Mavrikakis, *Surf. Sci.*, 2012, **606**, 679–689.
62 J. Strömquist, L. Bengtsson, M. Persson and B. Hammer, *Surf. Sci.*, 1998, **397**, 382–394.
63 S. Y. Lee, W. S. Yun and J. D. Lee, *ACS Appl. Mater. Interfaces*, 2017, **9**, 7873–7877.
64 M. Brandbyge, J.-L. Mozos, P. Ordejón, J. Taylor and K. Stokbro, *Phys. Rev. B: Condens. Matter Mater. Phys.*, 2002, **65**, 165401.
65 S. C. Miller Jr. and R. Good Jr., *Phys. Rev.*, 1953, **91**, 174.
66 R. Quhe, Y. Wang, M. Ye, Q. Zhang, J. Yang, P. Lu, M. Lei and J. Lu, *Nanoscale*, 2017, **9**, 14047–14057.
67 M. Farmanbar and G. Brocks, *Adv. Electron. Mater.*, 2016, **2**, 1500405.
68 M. Farmanbar and G. Brocks, *Phys. Rev. B: Condens. Matter Mater. Phys.*, 2015, **91**, 161304.
69 J. Su, L. Feng, W. Zeng and Z. Liu, *Phys. Chem. Chem. Phys.*, 2016, **18**, 31092–31100.
70 J. Su, L.-p. Feng, X. Zheng, C. Hu, H. Lu and Z. Liu, *ACS Appl. Mater. Interfaces*, 2017, **9**, 40940–40948.